# Floquet topological transition by unpolarized light

Bhaskar Mukherjee
*Theoretical Physics Department, Indian Association for the Cultivation of Science, Jadavpur, Kolkata 700032, India*

(Received 22 August 2018; revised manuscript received 20 November 2018; published 6 December 2018; corrected 6 March 2019)

We study Floquet topological transition in irradiated graphene when the polarization of incident light changes randomly with time. We numerically confirm that the noise-averaged time-evolution operator approaches a steady value in the limit of exact Trotter decomposition of the whole period during which incident light has a different polarization at each interval of the decomposition. This steady limit is found to coincide with the time-evolution operator calculated from the noise-averaged Hamiltonian. We observe that at the six corners (Dirac $K$ point) of the hexagonal Brillouin zone of graphene random Gaussian noise strongly modifies the phase band structure induced by circularly polarized light, whereas in the zone center ($\Gamma$ point) even a strong noise is not able to do the same. This can be understood by analyzing the deterministic noise-averaged Hamiltonian, which has a different Fourier structure as well as a lower number of symmetries compared to the noise-free one. In one-dimensional systems noise is found to renormalize only the drive amplitude.

DOI: 10.1103/PhysRevB.98.235112

## I. INTRODUCTION

Realizing topological phenomena in solid-state systems has been one of the major topics in condensed-matter physics since the discovery of integer quantum Hall effect (IQHE) in two-dimensional (2D) semiconductor devices [1]. These materials are the model system for a 2D noninteracting electron gas which under the application of a strong magnetic field forms highly gapped Landau levels. This results in very precise quantization of Hall conductance [2,3] at low temperature and supports robust conducting chiral states at the edges [4,5]. Later, it was shown that the magnetic field is not necessary, and one can also observe such a phenomenon in systems described by tight-binding Hamiltonians [6]. The so-called Haldane model describe electrons hopping in a honeycomb lattice threaded by periodic magnetic flux with zero net flux. The resulting complex hopping is difficult to implement experimentally, and it was only recently that the advancement in ultracold atomic systems has made such experiments possible [7]. To avoid such complicated implementation of the Haldane model and thus realize Chern insulating states more easily, a possible alternative way, namely, irradiation of an electromagnetic wave on graphene, was proposed recently to achieve the essential goal of time-reversal symmetry breaking.

Graphene is a gapless 2D Dirac system [8] in which the gap closes linearly at all six corners of the hexagonal Brillouin zone (BZ), known as Dirac points. Out of these six points only two are inequivalent; they are termed $K$ and $K'$ and are related to each other by time-reversal symmetry. All other Dirac points can be obtained from these two points via translation by reciprocal lattice vectors. The gap is maximum ($6\gamma$, where $\gamma$ is the nearest-neighbor hopping strength) at the center of the BZ, known as the $\Gamma$ point, and hence determines the bandwidth of the graphene spectrum. Controlled manipulation of the band structure, for example, opening up a gap at the Dirac points, is necessary for device applications. Research in these directions shows that growing the graphene sample on SiC [9], BN, etc., can open up a gap by breaking the sublattice symmetry. This kind of gap, known as a trivial gap, can be modeled by adding a constant (Semenoff) mass term in the tight-binding Hamiltonian which produce Berry curvature of opposite sign around $K$ and $K'$ and thus give a zero Chern number when integrated over the full BZ. Intrinsic spin-orbit coupling (SOC) produces a $Z_2$ topological order in the graphene band structure by restoring time-reversal symmetry [10,11]. Unfortunately, in pristine graphene this gap is too small to observe the proposed quantum spin Hall (QSH) phase even at very low temperature. There are some first-principles studies showing significant enhancement of this SOC gap (up to $\approx$20 meV) by growing the graphene sample on heavy compounds like $Sb_2Te_3$ [12], but this enhanced gap is still lower than room temperature ($\approx$25 meV).

It was proposed that explicit violation of time-reversal symmetry by irradiation of circularly polarized light on graphene can also open up a nontrivial gap at the Dirac point, turning it into a Haldane-Chern insulator [13,14]. In the experimentally accessible regime [15] this gap ($\approx$53 meV) is already higher than room temperature and is further tunable by controlling the light intensity and frequency. This resulting new state, termed the Floquet topological insulator, was found later in many other systems [16,17]. It is also detectable by various transport signatures [18–20]. Smooth variation of the polarization-controlling phase angle in real space can be used to manipulate several properties of these systems, including generation of fractionalized excitations [21]. These are steady states of periodically driven nonequilibrium systems [22–26] which recently gained tremendous attention because of their potential to create new phases which can hardly be found in their equilibrium counterparts. Traditional bulk-boundary correspondence was extended to Floquet topological systems taking into account the periodicity of the Floquet spectrum [27,28]. Experimental verification of such states has already been achieved using both time- and angle-resolved

 

photoemission spectroscopy (ARPES) [15,29] and also in photonic systems [30,31].

Throughout the past decade a large number of studies of real-time dynamics in closed quantum systems have extended the notions of universality from equilibrium to nonequilibrium via Kibble-Zurek scaling [32]. Further studies showed that the qualitative nature of these scalings can be completely reversed by introducing noise in the drive [33]. In these studies the Heisenberg equation of motion picks up a dephasing term due to averaging over different noise realizations, which leads to nonunitary dynamics. Recently, in equilibrium systems it was shown that periodicity in space (i.e., the crystal structure) is not necessary to get topological behavior and one can also see it in amorphous systems [34]. Analogously, one can ask at this point what would happen in Floquet systems if time periodicity of the Hamiltonian is broken due to the presence of noise in the drive. Several studies in this direction in models decomposable in free fermions already revealed that the nature of the asymptotic steady state depends on the type of aperiodic protocol [35]. Further, some analytical studies showed that disorder averaging can be avoided for a special class of protocols [36].

Influenced by this kind of work, we plan to study the fate of the Floquet topological systems when the smooth time variation of an incident electromagnetic wave is broken by the insertion of a random phase in one of the components of the vector potential. This kind of noise is always there in a typical experiment if the setup to produce polarized light is not calibrated properly. Moreover, such a noisy vector potential can also be generated artificially using synthetic gauge fields. We call this kind of monochromatic wave unpolarized light in the sense that the associated Lissajous figures keep on changing with time. The central results of this work can be summarized as follows. We show that depending on the spatial dimension of the problem Floquet topological transitions can be influenced by the random change in polarization of incident light. For graphene we find that the transitions at the Dirac ($K$) point are significantly modified compared to those at the $\Gamma$ point. The origin of this effect can be understood to be due to a fundamental change in the Fourier structure of the noise-averaged time-dependent Hamiltonian at the $K$ point. At low frequencies of the incident radiation, it is well known that symmetries of the underlying Hamiltonian are crucial for topological transition [37]. In the presence of noise, we find such symmetries to be broken. Interestingly, in contrast to the standard expectation, we find that few of these symmetries are restored in the noise-averaged Hamiltonian. This symmetry restoration has an impact on the self-averaging limit in this parameter regime. Finally, for a one-dimensional (1D) model ($p$-wave superconducting wire), using a nontrivial drive protocol, we show that even a strong noise (large standard deviation) cannot prohibit the transition.

The rest of this paper is structured as follows. In Sec. II we introduce our protocol for irradiated graphene and plot the results (phase bands) for numerical disorder averaging. In Sec. II A we establish the existence of the self-averaging limit, which suggests numerical averaging is meaningful and can be mimicked by the ensemble-averaged Hamiltonian. This is followed by a possible explanation of the deviation from noise-free (the circularly polarized case) behavior separately in high- and low-frequency regimes in Secs. II B and II C, respectively. Next, in Sec. III, we show results for 1D systems. Finally, we conclude and discuss possible experimental scenarios in Sec. IV.

## II. IRRADIATED GRAPHENE

We consider graphene irradiated by an electromagnetic wave defined by the vector potential $\mathrm{A} = A_0(\cos[\omega t + \phi(t)], \sin(\omega t))$. We have to further assume it to be space independent in the graphene plane to keep the integrability of the problem intact. The $\phi = 0$ (circularly polarized) case is well studied in the literature [38]. We allow $\phi$ to be a normally distributed random variable with mean $\mu$ and standard deviation $\sigma$ at each instant of time, which gives rise to its unpolarized nature. If one wishes to produce this vector potential in a laboratory, then this kind of noise will be inherently present as a random experimental error. The normalized probability distribution of $\phi$ at each time instant $t$ is given by

$$P(\phi) = \frac{1}{\sqrt{2\pi}\sigma} e^{-\frac{(\phi-\mu)^2}{2\pi\sigma^2}}, \tag{1}$$

where $\mu$ can be any real number within the interval $(-\pi \leqslant \mu \leqslant \pi)$. Here we will concentrate on the special value $\mu = 0$ (i.e., this is the value of $\mu$ in all plots), which will allow us to directly compare the result with circularly polarized case.

The time-dependent graphene Hamiltonian (for each $k$ mode) after Peierls's substitution with this protocol becomes

$$H(\mathrm{k}, t) = \begin{pmatrix} 0 & Z(\mathrm{k}, t) \\ Z^*(\mathrm{k}, t) & 0 \end{pmatrix}, \tag{2}$$

where $Z(\mathrm{k}, t) = -\gamma[2e^{i\frac{\tilde{k}_y}{2}}\cos(\frac{\sqrt{3}\tilde{k}_y}{2}) + e^{-i\tilde{k}_x}]$ and $\tilde{\mathrm{k}} = \mathrm{k} + e\mathrm{A}$.

Next, we calculate the time-evolution operator over one time period $T$ for each $k$ mode by dividing the period into $N$ parts,

$$\begin{aligned} U_k(T, 0) &= T_t e^{-i\int_0^T H_k(t')dt'} \\ &= e^{-iH_k(T-\delta t)\delta t} e^{-iH_k(T-2\delta t)\delta t} \cdots e^{-iH_k(2\delta t)\delta t} \\ &\quad \times e^{-iH_k(\delta t)\delta t}, \end{aligned} \tag{3}$$

where $T_t$ denotes the time-ordered product and $\delta t = T/N$ is a very small but fixed time interval. Such decomposition introduces Trotter error, which gets reduced with increasing $N$ and reproduces the exact $U$ for the chosen continuous drive in the $N \to \infty$ limit. We calculate the time-dependent Hamiltonian at each partition by drawing $\phi$ from a normal distribution and, using Eq. (3), get $U(T, 0)$ for one particular noise realization. We then average over several such realizations numerically and get the noise-averaged time-evolution operator

$$\langle U_k(T, 0)\rangle = \left\langle T_t e^{-i\int_0^T H_k(t')dt'}\right\rangle. \tag{4}$$

Equation (4) has a self-averaging limit [39] in the sense that all four elements of $\langle U(T, 0)\rangle$ go to some steady value with increasing the number of partitions $N$. We shall discuss this in more detail in the next section.

In Fig. 1 we plot the phase bands $\Phi(T)$ obtained using $\cos[\Phi(T)] = \mathrm{Re}[\langle U(T)\rangle_{11}]$. We can see that with increasing the magnitude of random noise the phase bands get modified, but we recover the results for pure circularly polarized light

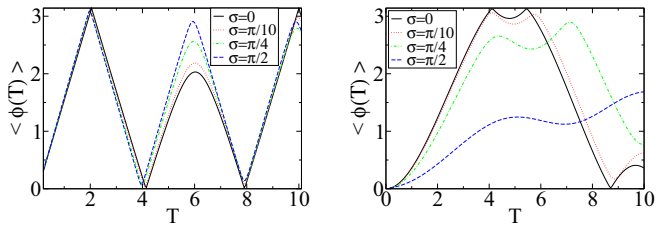


FIG. 1. Noise-averaged phase bands vs $T$ for the Γ point (left; at $\alpha = 1.5$) and for the $K$ point (right; at $\alpha = 2.0$) for various values of standard deviation $\sigma$. $N = 1000$, the number of samples is 1000, and $\alpha = eA_0/c$.

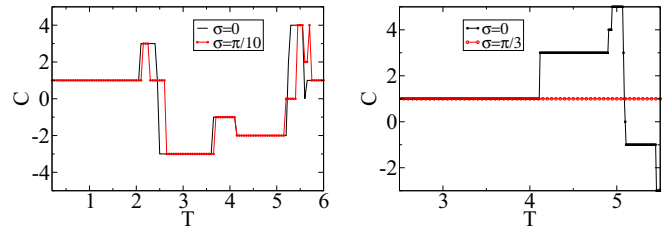


FIG. 2. Chern number of the noise-averaged lower Floquet band, showing the transitions through the Γ (left) and $K$ (right) points. Others parameters are the same as in Fig. 1.

in the $\sigma \to 0$ limit as expected. We find that the phase bands remain almost unchanged for the Γ point for a broad range of parameter values; however, at the $K$ point, they are strongly modified by the noise. We calculate the Chern number of the lower Floquet band using the eigenfunctions of $\langle U(T)\rangle$ in a discretized Brillouin zone. The plot is shown in Fig. 2. We find that the transitions (the position of the integer jump in the Chern number) can sustain an appreciable amount of temporal noise and merely get shifted in parameter space, but very strong noise (large $\sigma$) abolishes them.

### A. Ensemble-averaged Hamiltonian

In this section we explore the possibility of constructing a deterministic Hamiltonian such that the time-evolution operator constructed using it resembles the noise-averaged time-evolution operator. In a recent work [39] Lobejko *et al.* showed rigorously that the difference between the ensemble-averaged time-evolution operator and the time-evolution operator constructed by the ensemble-averaged Hamiltonian scales as $O(\frac{1}{N})$ for a certain class of protocols. For these protocols the ensemble-averaged Hamiltonian at two different times commutes, which they termed "commutation in statistical sense." They further extended the applicability of the above theorem to some simple noncommuting Hamiltonian by numerical simulations. But unlike those cases, irradiated graphene contains the noise term within the argument of complicated trigonometric functions. Hence, the ensemble-averaged Hamiltonian cannot be obtained here simply by substituting $\phi$ by its mean value. Therefore, we explicitly calculate the ensemble-averaged Hamiltonian for irradiated graphene at time $t$,

$$\langle H_k(t)\rangle = \int_{-\infty}^{\infty} P(\phi) H_k(\phi, t) d\phi, \tag{5}$$

with the $P(\phi)$ given in Eq. (1) we get using Jacobi-Anger relations [40].

$$\langle Z(\mathrm{k}, t)\rangle = -\gamma\left(2e^{i\frac{k_x}{2}}\cos\left(\frac{\sqrt{3}[k_y + \alpha\sin(\omega t)]}{2}\right)\left\{J_0\left(\frac{\alpha}{2}\right) + 2\sum_{n=1}^{\infty} i^n J_n\left(\frac{\alpha}{2}\right)e^{-\frac{n^2\sigma^2}{2}}\cos[n(\omega t + \mu)]\right\}\right.$$
$$\left. + e^{-ik_x}\left\{J_0(\alpha) + 2\sum_{n=1}^{\infty}(-i)^n J_n(\alpha)e^{-\frac{n^2\sigma^2}{2}}\cos[n(\omega t + \mu)]\right\}\right) \tag{6}$$

Using this, we numerically calculate the Frobenius norm of the distance between $\langle U(H(t))\rangle$ and $U(\langle H(t)\rangle)$,

$$D_N = \left|\left|\left\langle T_t e^{-i\int_0^T H(t')dt'}\right\rangle - T_t e^{-i\int_0^T \langle H(t')\rangle dt'}\right|\right|, \tag{7}$$

and the same norm for the corresponding variance matrix,

$$S_N = \left|\left|\left\langle\left(T_t e^{-i\int_0^T H(t')dt'} - T_t e^{-i\int_0^T \langle H(t')\rangle dt'}\right)^2\right\rangle\right|\right|, \tag{8}$$

where $N$ is the number of partitions used to calculate [using Eq. (3)] each quantity inside the norm. These are two appropriate quantities to measure the deviation of the time-evolution operator in different noise realizations. We see the power law decrease of both $D_N$ and $S_N$ in the number of partitions $N$ (see Fig. 3), which suggests a self-averaging limit exists here. It is only in this limit that the disorder averaging is meaningful in dynamical systems in the sense that the final results will depend on only the disorder parameters (mean, standard deviation, etc.) and not on different realizations. This is in close analogy to systems with spatial disorder where for each disorder realization some amount of deviation (from the mean) is introduced in all physical observables due to the finite size of the system but these deviations get canceled when averaged out over several disorder realizations and thus help to achieve the thermodynamic result quickly. Here in a dynamical system a finite number of partitions $N$ plays the role of finite system size, and the thermodynamic limit corresponds to the continuous drive ($N \to \infty$). The vanishing of $S_N$ with large $N$ also implies the equivalence

$$\cos[\langle\Phi(T)\rangle] \equiv \langle\cos[\Phi(T)]\rangle, \tag{9}$$

which we have used throughout the paper. In Fig. 3 note that $D_N$ and $S_N$ have larger values at the $K$ point compared to the Γ point for small $N$. This is related to the fact that the time-dependent Hamiltonian of irradiated graphene at the $K$ point is more complicated than at the Γ point due to the

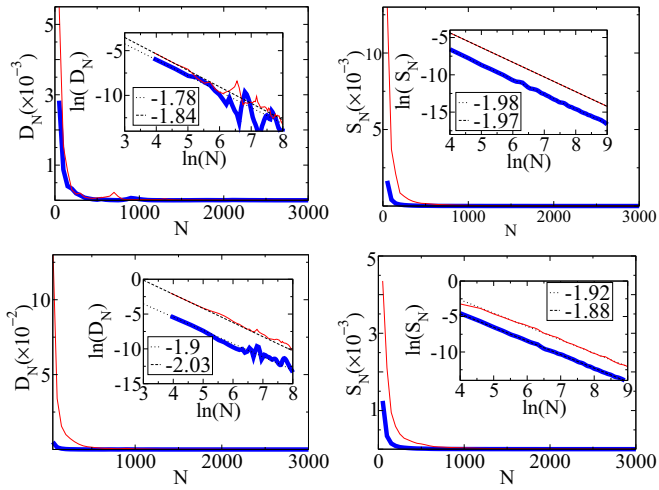


FIG. 3. Decrease of $D_N$ (top left panel) and $S_N$ (top right panel) with $N$ for the Γ point at $\alpha = 1.5$ and $T = 4.0$. The same is shown for the Dirac point in the lower left and right panels at $\alpha = 2$ and $T = 4.0$. The number of samples is 1000, and $\sigma$ is $\pi/10$ and $\pi/3$ for the thick blue and think red curves, respectively. The slope of the linear fit is mentioned in the insets.

presence of fewer symmetries [37]. The larger the complexity is, the larger the $N$ one needs to use to reduce these errors is. This power law decrease suggests that the time-consuming numerical disorder averaging can be avoided with the use of an ensemble-averaged Hamiltonian to calculate $U(T, 0)$ with a sufficiently large number of partitions of the whole period. We further demonstrate this by explicitly comparing the phase bands from both these methods in Fig. 4. Our next target is to understand better why in some cases weak noise is sufficient to modify the photoinduced gaps (as in the $K$ point) but in some other cases (as in the Γ point) even a strong noise cannot do the same. We will carry out this research by analyzing the ensemble-averaged Hamiltonian [Eq. (6)] in two different frequency regimes.

### B. High-frequency Floquet formalism

The Floquet formalism allows one to treat a periodic time-dependent problem as a time-independent eigenvalue problem. The cost of this is to deal with an infinite-dimensional Hilbert space (known as Sambe space) which is a direct product of the original Hilbert space and the space of $T$-periodic functions. The representation of the Floquet Hamiltonian [related to $U(T, 0)$ by $U(T, 0) = e^{-iH_F T}$] in this basis

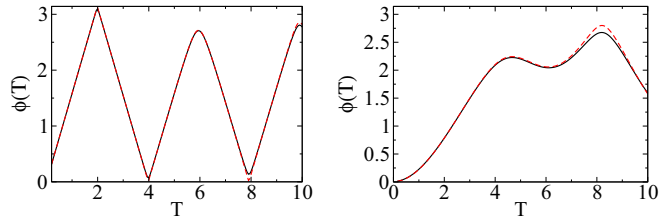


FIG. 4. Comparison of phase bands obtained by numerically disorder averaging the $U(T, 0)$ operator (black solid line) and by using the ensemble-averaged $H(t)$ to calculate the $U(T, 0)$ operator (red dashed line) for the Γ point (left panel) and for the $K$ point (right panel). The relevant parameters are the same as in Fig. 3.

is defined by the following matrix elements:

$$H^{m,n}_{i,j} = m\omega\delta_{mn}\delta_{ij} + \frac{1}{T}\int_0^T e^{-i(m-n)\omega t'} H_{ij}(t')dt', \qquad (10)$$

where $(m, n)$ is the row and column index of different square blocks each of size $(H_1 \times H_1)$, where $H_1$ is the Hilbert space dimension of the equilibrium problem (2 for each $k$ mode in our case), and $(i, j)$ denotes the position of each matrix element within one such block. For numerical purposes one can truncate this matrix after some order which depends on the details of the problem, especially the absolute value of the maximum order of the Fourier components (of the time-dependent Hamiltonian) with a nonvanishing coefficient. One also needs to increase the truncation dimension with decreasing frequency. Following this prescription, one can safely truncate the Floquet Hamiltonian for the noise-free case in the zeroth order at the Γ point(where one has a $2 \times 2$ $H_F$) and in the first order at the $K$ point (where one has a $6 \times 6$ $H_F$) for high frequencies and a low amplitude of radiation [13,38]. Thus, one gets expressions for the Floquet conduction band $\Phi(T)$ in the first quasienergy BZ for the noise-free (circularly polarized) case with the hopping amplitude $\gamma$ set to unity:

$$\Phi(\Gamma, T) = 3J_0(\alpha)T, \qquad (11)$$

$$\Phi(K, T) = \frac{\sqrt{4\pi^2 + 36J_1^2(\alpha)T^2} - 2\pi}{2}. \qquad (12)$$

Next, we aim to calculate some simplified expression of the phase band for the unpolarized light using the ensemble-averaged Hamiltonian in some suitable parameter regime. We can sufficiently simplify Eq. (6) for strong noise. Note that although $\phi$ appears to be an argument of trigonometric functions due to its random nature at each instant of time, $\phi[\mu, \sigma]$ and $\phi[\mu + 2n\pi, \sigma + 2p\pi]$ will not give the same time-evolution operator. Using $e^{-\frac{n^2\sigma^2}{2}} \approx 0$ for large $\sigma$ in Eq. (6), we get

$$\langle Z(\mathrm{k}, t)\rangle\ |_{\sigma\gg 0} \approx -\gamma\left[2J_0\left(\frac{\alpha}{2}\right)e^{ikx}\cos\left\{\frac{\sqrt{3}}{2}[ky + \alpha\sin(\omega t)]\right\} + J_0(\alpha)e^{-ikx}\right]; \qquad (13)$$

for the Γ point this gives a Hamiltonian proportional to only $\sigma_x$, and hence, we simply get the phase band

$$\Phi(\Gamma, T) = \int_0^T \langle Z(\Gamma, t')\rangle dt'. \qquad (14)$$

The integrand is difficult, but again using Jacobi-Anger relations, we get (taking $\gamma = 1$)

$$\Phi(\Gamma, T) = \left[2J_0\left(\frac{\alpha}{2}\right)J_0\left(\frac{\sqrt{3}\alpha}{2}\right) + J_0(\alpha)\right]T + 4J_0\left(\frac{\alpha}{2}\right)\sum_{n=1}^{\infty} J_{2n}\left(\frac{\sqrt{3}\alpha}{2}\right)\int_0^T \cos(2n\omega t')dt'$$
$$= \left[2J_0\left(\frac{\alpha}{2}\right)J_0\left(\frac{\sqrt{3}\alpha}{2}\right) + J_0(\alpha)\right]T. \tag{15}$$

Similarly, for the $K$ point we get

$$\Phi(K, T) = \left[J_0(\alpha) - J_0\left(\frac{\alpha}{2}\right)J_0\left(\frac{\sqrt{3}\alpha}{2}\right)\right]T; \tag{16}$$

we compare cosines of Floquet bands for the circularly polarized ($\sigma = 0$) and unpolarized ($\sigma \gg 0$) cases in Fig. 5. The functional behavior of these two bands does not change much for the $\Gamma$ point, whereas for the $K$ point they show drastically different behaviors. This huge change for the $K$ point is due to the fact that strong noise (highly unpolarized light) changes the lowest nonvanishing Fourier component of $\langle H_K(t)\rangle$ from 1 to 0 and thus reduces the effective Sambe space dimension from 6 to 2. These changes make the Floquet band at the $K$ point depend on only $J_0$, abolishing $J_1$. Note that $J_0$ and $J_1$ have completely different behaviors when the argument is small; the former is a decreasing function, but the latter is an increasing function of the argument.

### C. Low frequency

At low frequencies (and also at high radiation amplitudes) one need to take into account the higher Fourier components of the time-dependent Hamiltonian, and consequently, the truncation dimension of the Floquet Hamiltonian increases. This is why at low frequencies one cannot have a simple analytical expression of Floquet bands in terms of Bessel functions, and one needs to consider other methods like the adiabatic impulse which matches well with numerics in low to moderate frequencies and at high amplitudes [37]. Symmetries of $H(t)$ also play a crucial role in predicting the existence of phase band crossings at different high-symmetry points. But before going into the details of that we investigate the behavior of $D_N$ and $S_N$ as a function of $N$ at low frequencies. Generally, low $\omega$ and hence a high period $T$ necessitate a proportional increase of the number of partitions, but numerics suggests that the convergence of these quantities to zero is much slower than that in this parameter regime. In Fig. 6 (top left, top right, and bottom left panels) we demonstrate this. We see for a typical high $\sigma$ one needs to increase $N$ nearly quadratically (instead of linearly) with $T$ to make the value of $D_N$ go below some particular threshold. We therefore, to reduce the numerical cost, keep all our calculations confined within small $\sigma$ values at low frequencies.

It was shown in Ref. [37] that there exists sixfold symmetries at the $\Gamma$ point of graphene irradiated by circularly polarized (CP) light. This was shown to be responsible for phase bands crossing simultaneously at $T/3$, $2T/3$, and $T$. But here for unpolarized light, typically, all these symmetries are absent for any disorder realization. Consequently, disorder averaging also leads to avoided crossing. Here also the ensemble-averaged Hamiltonian can capture the essential physics, but interestingly, two of the symmetries get restored in it. We chart out the symmetries of the $\Gamma$ point under the irradiation of CP and unpolarized [ensemble-averaged $H(t)$] light in detail in Table I. This kind of symmetry mismatch between the two quantities inside the norm of Eq. (7) has a significant impact on the decrease of $D_N$ at low frequencies. We find that $D_N$ decreases very slowly with $N$ (see Fig. 6) here.

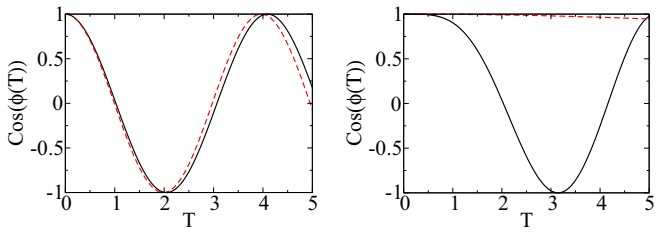


FIG. 5. Comparison of cosines of Eqs. (11) (black solid line) and (15) (red dashed line) for the $\Gamma$ point (left panel) and of Eqs. (12) (black solid line) and (16) (red dashed line) for the $K$ point (right panel). All parameters are the same as before.

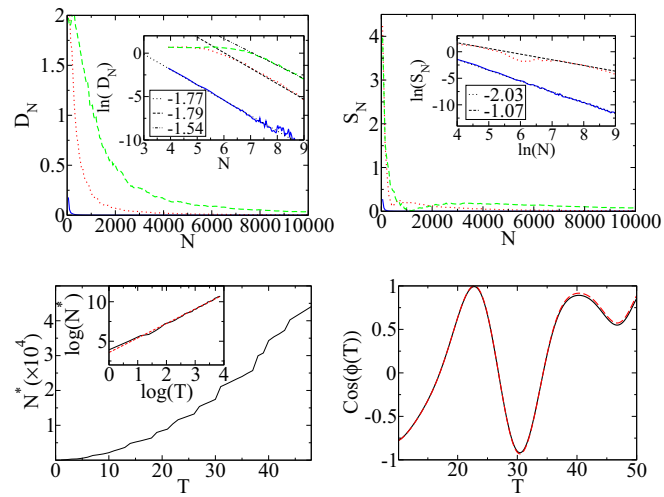


FIG. 6. Decrease of $D_N$ (top left panel) and $S_N$ (top right panel) with $N$ for the $\Gamma$ point at $\alpha = 2.0$ and $T = 60$. $\sigma$ for the blue solid, red dotted, and green dashed curves is $\pi/50$, $\pi/10$, and $\pi/3$ respectively. $N^*$ (for which $D_{N^*}$ fall below $10^{-4}$) vs $T$ is shown in the bottom left panel for $\sigma = \pi/3$. The slope of the linear fit in the log-log plot is 1.83 (inset). The bottom right panel shows the matching of the phase band from $\langle U(T)\rangle$ (black solid curve) and $U(T)$ calculated from $\langle H(t)\rangle$ (red dashed curve) for the $\Gamma$ point at $\alpha = 2.2$ and $\sigma = \pi/10$.

TABLE I. Symmetries of the Γ point for circularly polarized and unpolarized light.

| Symmetry | Type of polarization | |
|---|---|---|
| | CP | Unpolarized |
| $H(T-t)=H(t)$ | √ | √ |
| $H(\frac{T}{2}\pm t)=\tau_x H(t)\tau_x$ | √ | √ |
| $H(\frac{T}{6}\pm t)=\tau_x H(t)\tau_x$ | √ | X |
| $H(\frac{T}{3}\pm t)=H(t)$ | √ | X |
| $H(\frac{2T}{3}\pm t)=H(t)$ | √ | X |
| $H(\frac{5T}{6}\pm t)=\tau_x H(t)\tau_x$ | √ | X |

In Fig. 7 we show this symmetry mismatch between CP and unpolarized light [a large $\sigma$ is used for this purpose in Fig. 7(a)] and its consequences. Figure 7(b) shows (by exact numerical disorder averaging) a small $\sigma$ is sufficient to abolish the crossing at $T/3$. The same qualitative behavior is found when $\langle H(t)\rangle$ is used to calculate $U(T,0)$. We show in Figs. 7(c) and 7(d) that the crossings at $T/3$ and $2T/3$ get increasingly avoided with increasing $\sigma$.

## III. ONE-DIMENSIONAL SYSTEMS

One-dimensional interacting spin chains whose Hamiltonian can be expressed in terms of free fermions via Jordan-Wigner transformation have attracted a lot of theoretical attention in recent decades due to their integrable structure, the existence of topological transition, and the possibility of experimental realization using ion traps and ultracold atom systems. Nonequilibrium dynamics in these models is equally interesting because nontrivial topology can be induced by the

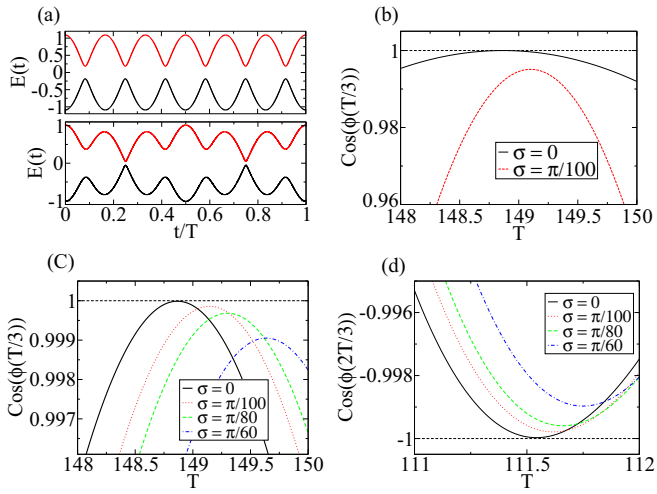


FIG. 7. (a) Instantaneous energies vs $t/T$ for CP (top panel) and for unpolarized ($\sigma=\pi/8$; bottom panel) light at the Γ point for $\alpha=2.3$. (b) $\cos[\Phi(\frac{T}{3})]$ vs $T$. The red curve is achieved by exact numerical averaging with 1000 samples, $N=10\,000$ for $\alpha=2.35$. (c) $\cos[\Phi(\frac{T}{3})]$ vs $T$ for $\alpha=2.35$. (d) $\cos[\Phi(\frac{2T}{3})]$ vs $T$ for $\alpha=2.28$. Phase bands in (c) and (d) are calculated using the ensemble-averaged Hamiltonian.

periodic drive of different terms in the Hamiltonian [41]. This can be independently done using multiple lasers with different amplitudes and frequencies. In these experiments phase differences between different drive terms can be randomly changed in the timescale $t_0 \ll 1/\omega$, where $\omega$ is the frequency of the drive. This constitutes a 1D platform to study physics similar to that studied in the previous section for 2D systems using unpolarized light. The survival of the topological transition under such a noisy drive is the key issue we would like to address. To this end, we consider a $p$-wave superconductor described by the following Hamiltonian [42,43]:

$$H=\sum_{i=1}^{L-1}[(\gamma c_i^\dagger c_i+\text{H.c.})+\Delta(c_i c_{i+1}+\text{H.c.})]$$
$$-\mu\sum_{i=1}^{L}(2c_i^\dagger c_i-1). \tag{17}$$

This model is equivalent to a spin-$\frac{1}{2}$ XY chain in a perpendicular magnetic field via Jordan-Wigner transformation [44]. After a Fourier transformation defined by $c_k=\frac{1}{L}\sum_{j=1}^{L}c_j e^{ikj}$ we can write this as

$$H=2\sum_{0\leqslant k\leqslant\pi}\psi_k^\dagger H_k\psi_k, \tag{18}$$

where $\psi_k=(c_k,c_{-k}^\dagger)^T$ is a two-component vector. Thus each $k$ mode of such systems can be described by the following Hamiltonian (we scale everything by $\gamma$):

$$H(k,t)=[\mu-\cos(k)]\sigma_z+\Delta\sin(k)\sigma_x, \tag{19}$$

and we use the following drive protocol: $\mu=A\cos[\omega t+\phi(t)]$ and $\Delta=\cos(r\omega t)$, where $r$ is an integer and $\phi$ is, as usual, a Gaussian random variable at each time $t$. The dynamics of this model is nontrivial for $r>1$ due to the nonremovable time dependence in both diagonal and off-diagonal elements [45,46]. This model [with $\phi(t)=0$] has a phase band crossing for $k=\pi/2$ at $t=T/2$ which exists at all frequencies. We study here what happens to this crossing if at each instant of time $\phi$ is a random Gaussian variable with zero mean. Below we mention the scheme for partitioning a full period to calculate the noise-averaged $U(t,0)$ now at any time $t\leqslant T$,

$$\delta t=\frac{t}{N}=\text{const}; \tag{20}$$

that is, we increase the number of partitions proportionally as the time $t$ gets closer to $T$, keeping the duration of the constant time evolution ($\delta t$) fixed. Thus, we calculate the noise-averaged phase band at all times $t$ within a period for different noise strengths $\sigma$ and compare it with the noise-free case in Fig. 8 (left panel). Interestingly, noise modifies the phase band at all times except at $t=T/2$, which is the phase band crossing point for the noise-free drive. This shows that the transition at $t=T/2$ is immune to any amount of temporal disorder. As a routine task we calculate the noise-averaged instantaneous Hamiltonian for the chosen protocol

$$\left\langle H\left(k=\frac{\pi}{2},t\right)\right\rangle=A\cos(\omega t)e^{-\sigma^2/2}\sigma_z+\cos(r\omega t)\sigma_x. \tag{21}$$

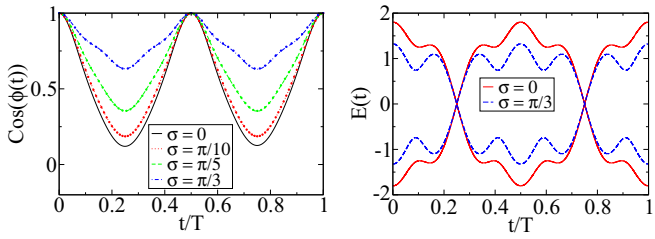


FIG. 8. Left: Phase bands from the numerically averaged $U$ operator (lines) and from the averaged Hamiltonians (dots) for the 1D model [in Eq. (17)]. $A = 1.5$, $\omega = 1.0$, $r = 3$. Right: The change in instantaneous energies with the insertion of noise.

In Fig. 8 (left panel) we see that time evolution governed by this averaged $H$ mimics the numerically disorder averaged $U$ operator like before. We note that this numerical agreement leads to the following statement: The effect of random noise is just to renormalize the laser amplitude,

$$\tilde{A} = Ae^{-\sigma^2/2}. \tag{22}$$

The robustness of the transition at $t = T/2$ also follows from the symmetry of Eq. (21). Note that the symmetry of the noise-free Hamiltonian for $k = \pi/2$ and for odd $r$ [namely, $H(T/2 - t) = -H(t)$] is not destroyed by the insertion of noise here (see Fig. 8, right panel). This can be used together with the Trotter-like decomposition of the $U$ operator [as in Eq. (3)] to show $U^{-1}(T/2) = U^{\dagger}(T/2) = U(T/2)$, signifying that a crossing through the Floquet zone center will always be there at $t = T/2$ for all parameter values ($A$, $\omega$, $\phi$, etc.). Further, the right panel of Fig. 8 demands that the same adiabatic-impulse method (as done for the noise-free case in Ref. [37]) can be used to show the existence of the crossing at $t = T/2$ in spite of the change in sizes of different adiabatic regions.

## IV. DISCUSSION

In this work we have studied the existence of the self-averaging limit in graphene irradiated by unpolarized light. We see the limit holds in the high-frequency regime and can be captured by the noise-averaged Hamiltonian. In low frequencies the limit is achieved very slowly as a possible consequence of retaining two of the symmetries in the noise-averaged Hamiltonian. This opens up an opportunity to search for some other deterministic Hamiltonian for speeding up the convergence to the asymptotic limit. We hardly found any steady limit at extremely low frequencies to the best of our numerical ability. Floquet topological transitions are found to be modified by the insertion of noise to various degrees depending on the $k$ point in the BZ. These range from a small shift in crossing positions to complete abolition of the transition depending on the amount of disorder. We found that certain $k$ points are more affected as a consequence of a change in the Fourier structure of their time-dependent Hamiltonian induced by the noise. The presence of a sixfold symmetry at the $\Gamma$ point plays a crucial role in the existence of a special type of crossing which simultaneously happens at $T/3$, $2T/3$, and $T$ [37]. This kind of crossing is ubiquitous at low frequencies but ceases to exist at high frequency (scanning the whole parameter regime as much as possible, we found they are absent below $T \approx 11$). Now breaking four of those six symmetries by the noise abolishes these transitions, confirming again the importance of symmetries at low frequencies. In 1D systems due to the simplicity of the BZ, noise obeys all symmetries of the clean time-dependent Hamiltonian, and as a consequence, crossings persist at all noise strengths. Noise merely renormalizes the drive amplitude.

In typical experiments one needs to keep the optical axis of a quarter-wave plate exactly at 45° with the plane of vibration of the incident plane polarized light to extract pure circularly polarized light. Now if this angle changes randomly (which is always the case to a small degree if the experiment is not performed carefully, such as a small vibration of the table on which the setup lies), then the polarization of the outgoing light will also fluctuate. A Babinet compensator is widely used to create an arbitrary phase difference between the ordinary ray and extraordinary ray in a broad spectral range. These two plane polarized light with mutually perpendicular plane of vibration are actually just the two component of the incident light inside such apparatus. One needs to get control over this on a timescale $\leqslant T$ to get the desired random change in polarization. One can also use synthetic gauge fields to produce such a noisy vector potential. This kind of perturbation is very common in an interference experiment if incoherent sources are used. The quantitatively different noise responses from various $k$ points can be experimentally verified by measuring the photoinduced gap in a momentum-resolved manner using pump-probe spectroscopy as done in Ref. [15]. The abolition of transition and hence a change in the topological structure of the Floquet bands can be detected by analyzing the intensity and angular dependence of ARPES spectra [29].

In conclusion we have shown random noise in the vector potential of incident light has a significant impact on the Floquet topological transition in graphene-like 2D systems. One can analyze the symmetries and Fourier structure of the noise-averaged Hamiltonian to understand the modifications caused by the noise. In 1D systems such noisy drives have no effect on the transitions.

## ACKNOWLEDGMENTS

The author thanks K. Sengupta and D. Sen for support and helpful discussions.

[1] K. V. Klitzing, G. Dorda, and M. Pepper, Phys. Rev. Lett. **45**, 494 (1980).
[2] R. B. Laughlin, Phys. Rev. B **23**, 5632 (1981).
[3] D. J. Thouless, M. Kohmoto, M. P. Nightingale, and M. den Nijs, Phys. Rev. Lett. **49**, 405 (1982).
[4] R. E. Prange, Phys. Rev. B **23**, 4802(R) (1981).
[5] B. I. Halperin, Phys. Rev. B **25**, 2185 (1982).
[6] F. D. M. Haldane, Phys. Rev. Lett. **61**, 2015 (1988).
[7] G. Jotzu, M. Messer, R. Desbuquois, M. Lebrat, T. Uehlinger, D. Greif, and T. Esslinger, Nature (London) **515**, 237 (2014).

[8] A. H. Castro Neto, F. Guinea, N. M. R. Peres, K. S. Novoselov, and A. K. Geim, Rev. Mod. Phys. **81**, 109 (2009).
[9] S. Y. Zhou, G.-H. Gweon, A. V. Fedorov, P. N. First, W. A. de Heer, D.-H. Lee, F. Guinea, A. H. Castro Neto, and A. Lanzara, Nat. Mater. **6**, 770 (2007).
[10] C. L. Kane and E. J. Mele, Phys. Rev. Lett. **95**, 226801 (2005).
[11] C. L. Kane and E. J. Mele, Phys. Rev. Lett. **95**, 146802 (2005).
[12] K.-H. Jin and S.-H. Jhi, Phys. Rev. B **87**, 075442 (2013).
[13] T. Oka and H. Aoki, Phys. Rev. B **79**, 081406 (2009).
[14] J.-I. Inoue and A. Tanaka, Phys. Rev. Lett. **105**, 017401 (2010).
[15] Y. H. Wang, H. Steinberg, P. Jarillo-Herrero, and N. Gedik, Science **342**, 453 (2013).
[16] N. H. Lindner, G. Refael, and V. Galitski, Nat. Physics **7**, 490 (2011).
[17] J. Cayssol, B. Dóra, F. Simon, and R. Moessner, Phys. Status Solidi RRL **7**, 101 (2013).
[18] T. Kitagawa, T. Oka, A. Brataas, L. Fu, and E. Demler, Phys. Rev. B **84**, 235108 (2011).
[19] A. Kundu and B. Seradjeh, Phys. Rev. Lett. **111**, 136402 (2013).
[20] I. Esin, M. S. Rudner, G. Refael, and N. H. Lindner, Phys. Rev. B **97**, 245401 (2018).
[21] Y. T. Katan and D. Podolsky, Phys. Rev. Lett **110**, 016802 (2013).
[22] L. D'Alessio and M. Rigol, Phys. Rev. X **4**, 041048 (2014).
[23] L. D'Alessio and M. Rigol, Nat. Commun. **6**, 8336 (2015).
[24] A. Lazarides, A. Das, and R. Moessner, Phys. Rev. E **90**, 012110 (2014).
[25] A. Lazarides, A. Das, and R. Moessner, Phys. Rev. Lett. **112**, 150401 (2014).
[26] A. Lazarides, A. Das, and R. Moessner, Phys. Rev. Lett. **115**, 030402 (2015).
[27] T. Kitagawa, E. Berg, M. Rudner, and E. Demler, Phys. Rev. B **82**, 235114 (2010).
[28] M. S. Rudner, N. H. Lindner, E. Berg, and M. Levin, Phys. Rev. X **3**, 031005 (2013).
[29] L. P. Gavensky, G. Usaj, and C. A. Balseiro, Sci. Rep. **6**, 36577 (2016).
[30] M. C. Rechtsman, J. M. Zeuner, Y. Plotnik, Y. Lumer, D. Podolsky, F. Dreisow, S. Nolte, M. Segev, and A. Szameit, Nature (London) **496**, 196 (2013).
[31] S. Mukherjee, A. Spracklen, M. Valiente, E. Andersson, P. Öhberg, N. Goldman, and R. R. Thomson, Nat. Commun. **8**, 13918 (2017).
[32] A. Polkovnikov, K. Sengupta, A. Silva, and M. Vengalattore, Rev. Mod. Phys. **83**, 863 (2011).
[33] A. Dutta, A. Rahmani, and A. del Campo, Phys. Rev. Lett. **117**, 080402 (2016).
[34] A. Agarwala and V. B. Shenoy, Phys. Rev. Lett. **118**, 236402 (2017).
[35] S. Nandy, A. Sen, and D. Sen, Phys. Rev. X **7**, 031034 (2017).
[36] U. Bhattacharya, S. Maity, U. Banik, and A. Dutta, Phys. Rev. B **97**, 184308 (2018).
[37] B. Mukherjee, P. Mohan, D. Sen, and K. Sengupta, Phys. Rev. B **97**, 205415 (2018).
[38] A. Kundu, H. A. Fertig, and B. Seradjeh, Phys. Rev. Lett. **113**, 236803 (2014).
[39] M. Lobejko, J. Dajka, and J. Luczka, Phys. Rev. A **98**, 022111 (2018).
[40] M. Abramowitz and I. A. Stegun, in *Handbook of Mathematical Functions with Formulas, Graphs, and Mathematical Tables*, Applied Mathematics Series. 55 (Dover Publications, Washington D.C., New York, 1983), Chap. 9, p. 355.
[41] M. Thakurathi, A. A. Patel, D. Sen, and A. Dutta, Phys. Rev. B **88**, 155133 (2013); M. Thakurathi, K. Sengupta, and D. Sen, *ibid.* **89**, 235434 (2014).
[42] A. Dutta, G. Aeppli, B. K. Chakrabarti, U. Divakaran, T. F. Rosenbaum, and D. Sen, *Quantum Phase Transitions in Transverse Field Spin Models: From Statistical Physics to Quantum Information* (Cambridge University Press, Cambridge, 2015).
[43] V. Mukherjee, U. Divakaran, A. Dutta, and D. Sen, Phys. Rev. B **76**, 174303 (2007); C. De Grandi and A. Polkovnikov, in *Quantum Quenching, Annealing, and Computation*, edited by A. K. Chan- dra, A. Das, and B. K. Chakrabarti, *Lecture Notes in Physics*, Vol. 802 (Springer, Heidelberg, 2010), p. 75.
[44] E. Lieb, T. Schultz, and D. Mattis, Ann. Phys. (N.Y.) **16**, 407 (1961).
[45] J. D. Sau and K. Sengupta, Phys. Rev. B **90**, 104306 (2014).
[46] S. Kar, B. Mukherjee, and K. Sengupta, Phys. Rev. B **94**, 075130 (2016).

*Correction:* A minor error in text in the definition of QSH in the Introduction has been fixed. A misprint introduced during the production process has been rectified in Eq. (3).